Numerical simulation on the NACA0018 airfoil self-noise generation

Min Jiang,[1] Xiaodong Li,[1, a)] Baohong Bai,[1] and Dakai Lin[2]
[1)] *Beihang University, Beijing 100191, China*
[2)] *Beijing Aeronautical Science and Technology Research Institute of COMAC, Beijing 100191, China*

(Received 5 May 2012; accepted 18 July 2012; published online 10 September 2012)

Abstract Airfoil self-noise is a common phenomenon for many engineering applications. Aiming to study the underlying mechanism of airfoil self-noise at low Mach number and moderate Reynolds number flow, a numerical investigation is presented on noise generation by flow past NACA0018 airfoil. Based on a high-order accurate numerical method, both the near-field hydrodynamics and the far-field acoustics are computed simultaneously by performing direct numerical simulation. The mean flow properties agree well with the experimental measurements. The characteristics of aerodynamic noise are investigated at various angles of attack. The obtained results show that inclining the airfoil could enlarge turbulent intensity and produce larger scale of vortices. The sound radiation is mainly towards the upper and lower directions of the airfoil surface. At higher angle of attack, the tonal noise tends to disappear and the noise spectrum displays broad-band features. © *2012 The Chinese Society of Theoretical and Applied Mechanics.* [doi:10.1063/2.1205204]

Keywords direct numerical simulation, computational aeroacoustics, airfoil self-noise, broad-band features

The noise radiated from an airfoil embedded in a uniform incoming flow is referred to as airfoil self-noise. Airfoil self-noise, commonly heard from wind turbine, aircraft, helicopter rotors and various types of turbo-machineries, is produced by the interaction of the boundary layer and wake with the airfoil itself. Since such noise is an important noise source in many applications, the study of this phenomenon therefore has been an important research topic in the aeroacoustic community. Amiet's[1] classical trailing-edge noise theory is considered to be an attractive approach due to the fact that the far-field noise can be accurately predicted, provided the surface pressure difference. Based on a large experimental database, Brooks et al.[2] proposed five sound generation mechanisms responsible for the airfoil self-noise, among which trailing edge (TE) mechanism will dominate for most applications. Recent rapid advances in computational aeroacoustics, turbulence modeling and parallel computation, have made it possible for direct noise computation. Different approaches of solving unsteady Navier-Stokes equations, such as direct numerical simulation (DNS) and large eddy simulation (LES), have been resorted for directly computing airfoil self-noise. Sandberg et al.[3] performed DNS for direct noise computation of airfoil self-noise. Marsden et al.[4] conducted LES of the flow around a NACA0012 airfoil and associated sound. More recently, Tam and Ju[5,6] applied DNS technique to investigate the generation of airfoil tones at moderate Reynolds numbers.

The main objective of the present paper is to simulate the noise generation by flow over airfoils and investigate the characteristics of the aerodynamic noise at various angles of attack. DNS is performed of flow over NACA0018 airfoil at Reynolds number of $Re = 1.6 \times 10^5$. The mean flow characteristics are compared with the measurements of Nakano et al.[7] The spectrum and directivity of noise are then investigated at various angles of attack.

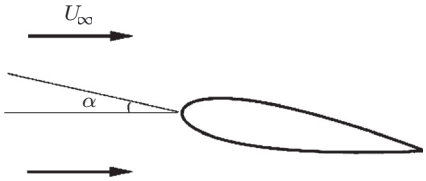

Fig. 1. Schematic diagram of the computational model.

A schematic diagram of the computational model is presented in Fig. 1. A symmetric NACA airfoil with a blunt trailing edge is placed in a uniform flow. NACA0018 airfoil is considered in this study. Here, U_∞ denotes the velocity of the uniform flow and C_∞ denotes the speed of sound. The lengths are made dimensionless by the chord width C of the airfoil. The velocity is scaled by the sound speed in ambient air of C_∞. The Reynolds number is defined as $Re = U_\infty C/\nu_\infty$, where ν_∞ is the kinematic viscosity. In this paper, the chord width of this airfoil is 80 mm and the velocity of the uniform flow is fixed at 30 m/s, which corresponds to a constant Reynolds number of $Re = 1.6 \times 10^5$. Much attention is paid to the effect of angle of attack on noise generation and radiation.

The problem of airfoil self-noise involves multi-scale physics. To be specific, a large length scale disparity exists between the viscous boundary layer and the sound propagation region far from the airfoil surface. All these scales need to be accurately resolved in the same simulation for the description of sound generation and propagation. Thus, the mesh should be elaborately designed. For these reasons, the multi-size mesh strategy is adopted in this study. Figure 2 shows

[a)] Corresponding author. Email: lixd@buaa.edu.cn.

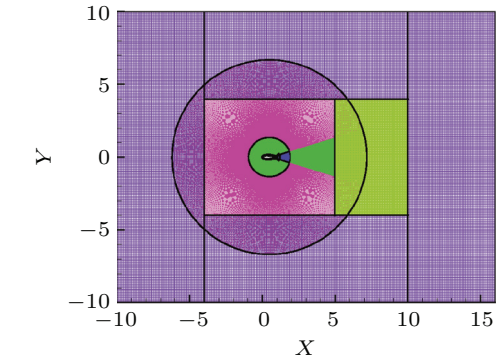

(a) Grid topology

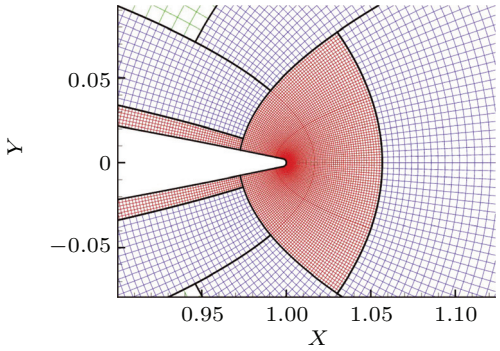

(b) Enlarged view of mesh around trailing edge

Fig. 2. Computational mesh (grid points are output every five points).

the multi-domain mesh for numerical simulation of the NACA0018 airfoil.

The flow under consideration is governed by the full compressible 2D Navier-Stokes equations. These equations are

$$\frac{\partial \rho}{\partial t} + \frac{\partial}{\partial x_k}(\rho u_k) = 0, \tag{1}$$

$$\frac{\partial}{\partial t}(\rho E) + \frac{\partial}{\partial x_k}\left[\rho u_k \left(E + \frac{p}{\rho}\right) - u_i \tau_{ik}\right] = 0. \tag{2}$$

The stress tensor is calculated as

$$\tau_{ik} = \frac{\mu}{Re}\left(\frac{\partial u_i}{\partial x_k} + \frac{\partial u_k}{\partial x_i} - \frac{2}{3}\frac{\partial u_j}{\partial x_j}\delta_{ik}\right). \tag{3}$$

Re is the Reynolds number based on chord width, and the molecular viscosity μ is calculated by Sutherland's law. Note that heat conduction is neglected in the energy equations.

The direct numerical computation of the flow and acoustics is performed to provide a full set of space-time data for Fourier transform analysis. The 2D governing equations are numerically solved by implementing high-order accurate schemes. For spatial derivatives, the 7-point dispersion-relation-preserving (DRP) scheme[8] is utilized with low dispersion and low dissipation for sound propagation. Considering the requirement of giant computation resource, a multi-size and multi-time step strategy[9] is implemented for the time

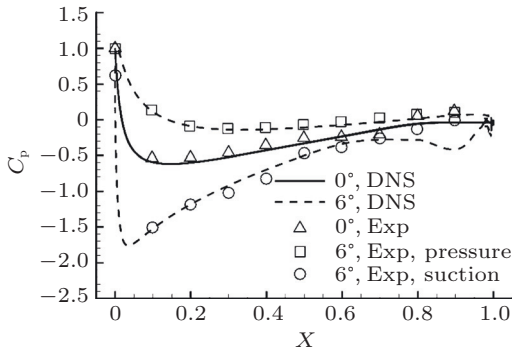

Fig. 3. Pressure coefficients C_∞ on airfoil surface.

integration. In this way, 70% of the CPU time is saved compared with applying single-time-step marching algorithm. The nonlinear perfectly matched layer (PML) boundary conditions proposed by Hu et al.[10] are applied around the computational domain. On the airfoil surface an adiabatic, no-slip boundary condition is imposed.

The time-averaged pressure coefficient is defined as $C_\mathrm{p} = 2(\bar{p} - p_\infty)/\rho_\infty U_\infty^2$, where $\bar{p}$ is the time-averaged pressure and ρ_∞ denotes the density of the uniform flow. The time-averaged pressure coefficient distributions at two angles of attack (0°, 6°) are plotted in Fig. 3. The results are measured from both the pressure and suction surface. For comparison, the experimental results[7] are also plotted in this figure. As shown in Fig. 3, the difference between our simulation and the experimental results is very small. It is also found that at zero attack angle the mean pressure coefficient distribution on two surfaces lies in one curve, which indicates that the results on pressure surface coincides with the one on suction surface. This is due to the symmetric feature of the flow about the airfoil axis. With an increase in attack angle to 6 degree, the pressure distribution becomes asymmetric. On the pressure surface, the pressure coefficient varies smoothly. While the pressure on the suction surface shows a sharp decrease just downstream the leading edge of the airfoil, and then increases gradually along the airfoil surface to form adverse pressure gradients. This process indicates that the large-scale separation has taken place on suction surface. Near the trailing edge there are some discrepancies between our simulation and experimental results. The pressure coefficient is found to be smaller than that measured from experiment, which is an implication that compared to the experiment the flow here has a larger velocity. This probably because that the simulation is performed using two dimensional model. While the real flow field is more complicated and totally three dimensional.

Figure 4 shows instantaneous vorticity field of the flow over a NACA0018 airfoil. When airfoil is horizontally set, vortices gradually form from the region near the airfoil surface and develop until well-defined vortices are formed beyond approximately one chord

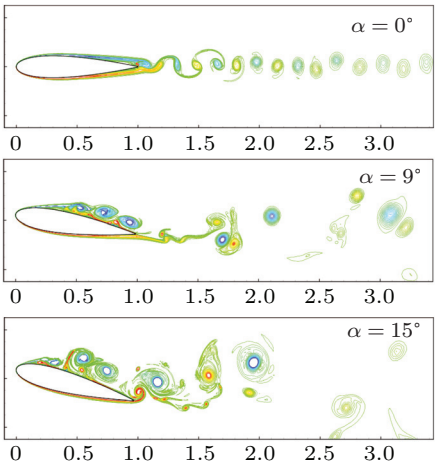

Fig. 4. Instantaneous vorticity field.

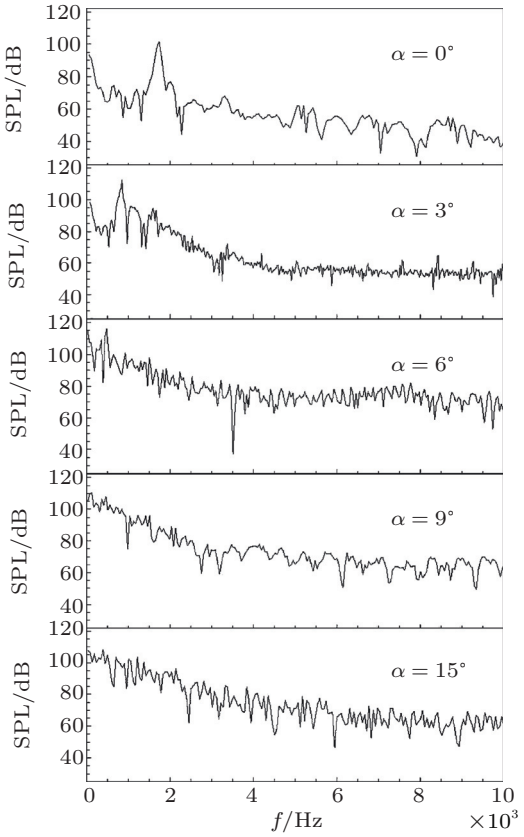

Fig. 5. Spectrum of aerodynamic noise.

width downstream of the trailing edge. These vortices are staggered aligned in the extended camber line of the airfoil. When airfoil is inclined to some extent, the flow starts to separate from the airfoil surface and vortices are observed to shed at the suction side and rolling downstream. Noise emerges accompanying with the separation and reattachment phenomenon. Further increase in angle of attack would result in the flow separation point moving upstream on the suction side and yielding larger scale of vortices. The combination and

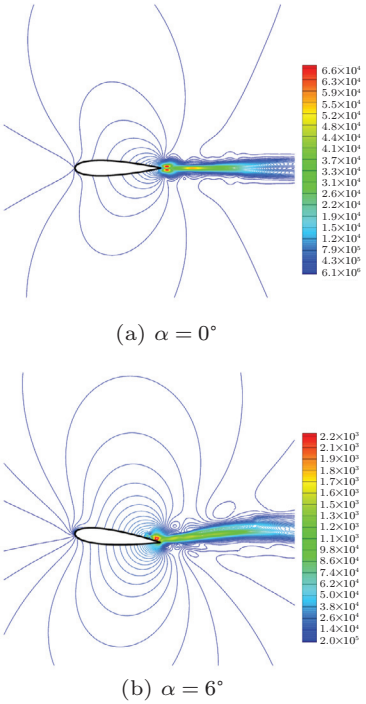

(a) $\alpha = 0°$

(b) $\alpha = 6°$

Fig. 6. Contours of root-mean-squared pressure fluctuations.

splitting of vortex pairs downstream the trailing edge also leads to noise generation and radiation. For very high angle of attack, the separated vortex structure is rather complicated and the separation point on suction surface is much closed to the leading edge.

Figure 5 shows the spectrum of aerodynamic noise measured from point $(x_A, y_A) = (0.3, 1.065)$ at various attack angles ranging from $\alpha = 0°$ to $\alpha = 15°$. At zero angle of attack, a prominent tone component is detected in the noise spectrum. The frequency of this tone in our simulation is 1 730 Hz, which approximately agrees with the result predicted by Paterson formula,[11] $f = 0.011 U_\infty^{1.5}/\sqrt{C\nu_\infty}$. Further increase in angle of attack leads to the gradual disappearance of the tonal noise and increase in magnitude of the noise level. At very high angle of attack, the noise spectrum is quite broader. This observation might be due to that with the increase in incidence, the flow over airfoil tends to be highly unsteady. For such highly unsteady flow, multi-scales vortices are produced in the wake and separation area. Thus, noise generated from the merging and splitting of these vortices probably exhibits wide band characteristics.

The root-mean-squared pressure fluctuation $p_{\rm rms}$ is somewhat considered as a measure of the strength of sound sources. In this paper, $p_{\rm rms}$ is therefore defined by the following way

$$p_{\rm rms} = \sqrt{\left(\int_0^T (p - \bar{p})^2 {\rm d}t\right)/T},$$

where p is the instantaneous pressure, $\bar{p}$ is the time-

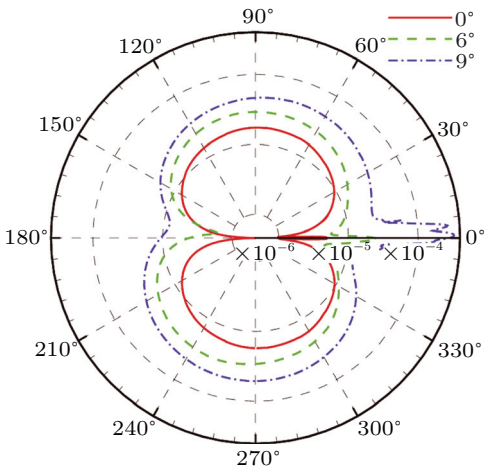

Fig. 7. Directivity patterns of root-mean-squared pressure fluctuations at $r = 5$.

averaged pressure and T denotes the integration time. In this study, the integration time T is more than 50.

The distribution of $p_{\rm rms}$, at $\alpha = 0°$ and $\alpha = 6°$ is shown in Fig. 6. The contour pattern is nearly symmetrical about the centerline of the wakes at zero incidence. When the angle of attack increases up to 6°, it becomes asymmetric. On examining these contours, the region around trailing edge and the wake flow are also found to have the highest value of $p_{\rm rms}$. Thus, the major sound sources responsible for noise radiation are generated in these regions.

Further investigations of the noise directivity features at three different angles of attack are reported in Fig. 7. This figure presents the directivities of $p_{\rm rms}$ measured along a circle of radius $r = \sqrt{(x-0.3)^2 + y^2} = 5$. It can be seen that for zero angle of attack, the directivity is nearly perfect symmetric about the axis of the airfoil. With rise in angle of attack, there is remarkable increase in the magnitude of radiated sound and increasing silt in the directivity pattern. Note that the silt direction is consistent with the trend of attack angle. The directivity is approximately a dipole source, but is not that of a point dipole placed in a uniform flow. The sound radiates mainly towards the upper and lower directions ($\theta = 90°$ and 270°) of the airfoil surface. Due to the vortex shedding, the sound radiation downstream ($\theta = 0°$) the trailing edge is still evident.

The direct numerical simulations were conducted of compressible flow over symmetric NACA0018 airfoil. High-order accurate numerical methods applied in this investigation enable precise description of the flow and sound field. Wake flow is nearly symmetric at low angles of attack and gradually becomes asymmetric when the airfoil is more inclined against the free stream. The increase in angle of attack would introduce larger scale of vortices and intensity of turbulence. At this low Mach number and moderate Reynolds number flow, the sound radiates mainly towards the upper and lower directions of the airfoil surface, which is demonstrated by the noise directivity plot. The frequency-domain analysis of pressure fluctuations indicates that the tonal noise gradually disappears when the angle of attack increases and the noise spectrum finally presents broad-band features.

This work was supported by the National Natural Science Foundation of China (10972022), the Specialized Research Fund for the Doctoral Program of Higher Education of China (20091102110011) and the 111 Projects B07009 of China.

1. R. Amiet, J. Sound Vib. **47**, 387 (1976).
2. T. Brooks, D. Pope, and M. Marcolini, NASA Reference Publication 1218, *NASA*, (1989).
3. R. D. Sandberg, L. E. Jones, and N. D. Sandham, et al., J. Sound Vib. **320**, 838 (2009).
4. O. Marsden, C. Bogey, and C. Bailly, AIAA J. **46**, 874 (2008).
5. C. K. W. Tam, and H. B. Ju, AIAA Paper **2006**, 2502 (2006).
6. C. K. W. Tam, and H. B. Ju, AIAA Paper **2011**, 2711 (2011).
7. T. Nakano, N. Fujisawa, and Y. Oguma, et al., J. Wind Eng. Industrial Aerodynamics **95**, 511 (2007).
8. C. K. W. Tam, and J. C. Webb, J. Comput. Phys. **107**, 262 (1993).
9. D. K. Lin, M. Jiang, and X. D. Li, J. Comput. Acoust. **201**, 1 (2010).
10. F. Q. Hu, X. D. Li, and D. K. Lin, J. Comput. Phys. **227**, 4398 (2008).
11. R. W. Paterson, P. G. Vogt, and M. R. Fink, J. Aircraft **10**, 296 (1973).